

The Effect of Large Scale Magnetic Turbulence on the Acceleration of Electrons by Perpendicular Collisionless Shocks

Fan Guo and Joe Giacalone

Department of Planetary Sciences, University of Arizona, Tucson, AZ 85721, USA

guofan@lpl.arizona.edu

Received _____; accepted _____

arXiv:1003.5946v1 [astro-ph.SR] 30 Mar 2010

ABSTRACT

We study the physics of electron acceleration at collisionless shocks that move through a plasma containing large-scale magnetic fluctuations. We numerically integrate the trajectories of a large number of electrons, which are treated as test particles moving in the time dependent electric and magnetic fields determined from 2-D hybrid simulations (kinetic ions, fluid electron). The large-scale magnetic fluctuations effect the electrons in a number of ways and lead to efficient and rapid energization at the shock front. Since the electrons mainly follow along magnetic lines of force, the large-scale braiding of field lines in space allows the fast-moving electrons to cross the shock front several times, leading to efficient acceleration. Ripples in the shock front occurring at various scales will also contribute to the acceleration by mirroring the electrons. Our calculation shows that this process favors electron acceleration at perpendicular shocks. The current study is also helpful in understanding the injection problem for electron acceleration by collisionless shocks. It is also shown that the spatial distribution of energetic electrons is similar to in-situ observations (e.g., Bale et al. 1999; Simnett et al. 2005). The process may be important to our understanding of energetic electrons in planetary bow shocks and interplanetary shocks, and explaining herringbone structures seen in some type II solar radio bursts.

Subject headings: acceleration of particles - cosmic rays - shock waves - turbulence

1. Introduction

Collisionless shocks are widely believed to be the primary acceleration mechanism giving rise to the ubiquitous existence of energetic particles in space. The theory of diffusive shock acceleration (DSA) was proposed some 30 years ago (Axford et al. 1978; Bell 1978; Blandford & Ostriker 1978; Krymsky 1977) and is currently believed to be the most important mechanism for a variety of astrophysical environments, for example, interplanetary shocks, the heliospheric termination shock, and shocks associated with supernova remnants. The theory predicts a universal power-law energy flux spectrum $dJ/dE \propto E^{-1}$ for strong shocks with a density compression ratio of 4.

The physical mechanism by which particles are accelerated from thermal energies to much higher energies where DSA is presumed to be applicable (the injection problem) has received some recent attentions but has not reached a common consensus explanation. Many acceleration theories, for example, shock drift acceleration (SDA) (see reviews, Armstrong et al. 1985; Decker 1988) and shock surfing acceleration (Sagdeev 1966; Lee et al. 1996; Zank et al. 1996) have been proposed. The acceleration of low energy protons in the shocks containing large-scale pre-existing magnetic fluctuations is very efficient (Giacalone 2005a,b), which suggests that there may not be an injection problem.

It is generally thought that, pre-accelerated particles will interact resonantly with magnetic turbulence which results in isotropization and diffusion. Many previous works considering magnetic turbulence focused on the ions (e.g., Bell 1978; Giacalone et al. 1992; Ng et al. 2003; Giacalone 2004, 2005a,b). However, the acceleration of electrons is less well understood since for electrons whose gyroradii are very small, the cyclotron resonance condition is not easily satisfied thus they cannot interact resonantly with large-scale ambient turbulence on ion-scale. While the scattering provided by whistler waves (Shimada et al. 1999) is one possibility, Jokipii & Giacalone (2007) proposed an attractive solution to

the injection problem that does not require pitch-angle scattering, i.e., conserving the first adiabatic invariant. The idea is that the low-rigidity particles, especially electrons, can move rapidly along meandering magnetic field lines and thus travel back and forth between shock front. The particles gain energy from the difference between upstream and downstream flow velocities.

Energetic electrons are often observed to be associated with collisionless shocks. Accelerated electrons are thought to produce type II radio bursts in the solar corona and interplanetary space. Anderson et al. (1979) reported *ISEE* spacecraft measurements of upstream electrons (> 16 keV) of the Earth’s bow shock that originate from a thin region close to the point of tangency between interplanetary magnetic field lines and the shock surface. Tsurutani & Lin (1985) showed observations of energetic electrons associated with interplanetary shocks showing ”spike-like” flux enhancements for energies $\gtrsim 2$ keV. The spike events were observed at quasi-perpendicular shocks with $\theta_{Bn} \gtrsim 70^\circ$, where θ_{Bn} is the angle between upstream magnetic field and shock normal. Some shock crossings had no enhancements of energetic electrons which were reported to be associated with low shock speeds and small θ_{Bn} . Simnett et al. (2005) presented data which shows energetic electrons are accelerated close to shock front. They also showed some accelerated electrons can escape far upstream of quasi-perpendicular interplanetary shocks. The clear evidence of electron acceleration by DSA is rare, but a recent example was discussed by Shimada et al. (1999) showing the importance of whistler waves.

In order to explain the energization of electrons within the shock layer, Wu (1984) and Leroy & Mangeney (1984) developed analytic models for electron acceleration from thermal energies by adiabatic reflection by a quasi-perpendicular shock. This is known as fast-Fermi acceleration. This theory describes a scatter-free electron acceleration process in a planar, time-steady shock. It obtains a qualitative agreement with observations at Earth’s bow

shock in terms of the loss-cone pitch-angle distribution and energy range of accelerated electrons. Krauss-Varban et al. (1989) used the combination of electron test particle simulation and 1-D hybrid simulation and verified Wu’s basic conclusions. The main energy source of fast Fermi acceleration comes from the $-\mathbf{V} \times \mathbf{B}/c$ electric field which is the same as SDA (Armstrong et al. 1985). It can also be demonstrated that fast-Fermi acceleration and SDA are the same process in two different frames of reference (Krauss-Varban & Wu 1989). Thus one would expect electrons to drift in the direction perpendicular to the flow and magnetic field. For a single reflection, the fraction and energies of accelerated particles are limited (e.g., Ball & Melrose 2001). Holman & Pesses (1983) proposed the basic outline for type II solar radio bursts in which energetic electrons are accelerated through SDA. It is expected that multiple reflections are required in order to explain herringbone structures in type II bursts, where the electrons are accelerated to a fraction of the speed of light. More recently, Burgess (2006) studied electron acceleration in 2-D quasi-perpendicular shocks using test-particle simulations and self-consistent hybrid simulations. He focused on the effect of the rippling of the shock front on particle acceleration in highly oblique shocks with $\theta_{Bn} \geq 80^\circ$. The ripples, in this case, were produced by instabilities along the shock front. Burgess found that the acceleration of electron by SDA can be more efficient for a rippled shock. The shape of the resulting energy spectra has a flat plateau from the initial release energies to energies several times higher than this. Above the flat plateau the spectra drop off steeply as θ_{Bn} become smaller.

In this paper, we use test particle simulations combined with 2-D hybrid simulations that include pre-existing large-scale magnetic field turbulence (Giacalone 2005b) to study the shock acceleration of electrons. In addition to the effect of the large-scale turbulence, the shock microphysics occurring on ion length and time scales is also included. Moreover, the shock front is rippled and distorted in response to the turbulence, which is also included in our model. In § 2 we describe the numerical method we used to combine the fields from

the hybrid simulation and test-particle simulation to obtain the electron distribution. § 3 gives the main results of our simulation. In § 4 we summarize the main conclusions and discuss the implication of our work.

2. Numerical Method

Investigating particle transport in the vicinity of a collisionless shock requires a spatial scale large enough for particles to propagate back and forth across the shock, and a spatial resolution small enough to include the detailed physics for particle scattering and shock microstructure. We implement a combination of a 2-D hybrid simulation to model the fields and plasma flow and a test particle simulation to follow the orbits of a large number of energetic electrons. In the first step, we employ a two-dimensional hybrid simulation similar to previous work (Giacalone 2005b) that includes pre-existing large-scale turbulence. In the hybrid simulation (e.g., Winske & Quest 1988), the ions are treated fully kinetically and thermal (i.e., non-energetic) electrons are treated as a massless fluid. This approach is well suited to resolve ion-scale plasma physics which is critical to describe supercritical collisionless shocks. In this study, we consider a two-dimensional Cartesian grid in the $x - z$ plane. All the physical vector quantities have components in three directions, but depend spatially only on these two variables. A shock is produced by using the so-called piston method (for a discussion, see Jones & Ellison 1991), in which the plasma is injected continuously from one end ($x = 0$, in our case) of the simulation box, and reflected elastically at the other end ($x = L_x$). This boundary is also assumed to be a perfectly conducting barrier. The pileup of density and magnetic field creates a shock propagating in the $-x$ direction. To include the large-scale magnetic fluctuations, a random magnetic field is superposed on a mean field at the beginning of the simulation and is also injected continuously at the $x = 0$ boundary during the simulation. The simplified one-dimensional

fluctuations have the form $\mathbf{B}(z, t) = \delta\mathbf{B}(z, t) + \mathbf{B}_1$, where \mathbf{B}_1 is the averaged upstream magnetic field. The fluctuating component contains an equal mixture of right- and left-hand circularly polarized, forward and backward parallel-propagating plane Alfvén waves. The amplitude of the fluctuations is determined from a Kolmogorov power spectrum:

$$P(k) \propto \frac{1}{1 + (kL_c)^{5/3}}$$

in which L_c is the coherence scale of the fluctuations, see (Giocalone 2005b) for more details. For the simulations presented in this study, we take $L_c = L_z$, which is the size of simulation box in z direction. Note that in addition to magnetic fluctuations, there are also velocity perturbations with $\delta\mathbf{v} = v_{A1}\delta\mathbf{B}/B_1$ (Alfvén waves). For most of the parts in the paper, we consider a turbulence variance $\sigma = \delta B^2/B_1^2 = \delta v^2/v_{A1}^2 = 0.3$, where δv and v_{A1} are the magnitude of velocity perturbation and upstream Alfvén speed, respectively. We also discuss the effect of different values of turbulence variances.

The size of the simulation box $L_x \times L_z = 400c/\omega_{pi} \times 1024c/\omega_{pi}$, where c/ω_{pi} is the ion inertial length. The Mach number of the flow in the simulation frame is $M_{A0} = 4.0$, the averaged Mach number in the shock frame is about 5.6. Most of the results presented here are for averaged shock normal angle $\langle \theta_{Bn} \rangle = 90^\circ$, but we also simulate the cases for $\langle \theta_{Bn} \rangle = 60^\circ$ and 75° to examine the dependence of the acceleration efficiency on shock normal angle. The other important simulation parameters include electron and ion plasma beta $\beta_e = 0.5$ and $\beta_i = 0.5$, respectively, grid sizes $\Delta x = \Delta z = 0.5c/\omega_{pi}$, time step $\Delta t = 0.01\Omega_{ci}^{-1}$, the ratio between light speed and upstream Alfvén speed $c/v_{A1} = 8696.0$, and the anomalous resistivity is taken to be $\eta = 1 \times 10^{-5}4\pi\omega_{pi}^{-1}$. The initial spatially uniform thermal ion distribution was generated using 40 particles per cell. Different from previous studies, the consideration of large-scale magnetic fluctuations enables us consider the effect of pre-existing magnetic turbulence on electron acceleration, which has been

shown to be important for low-energy ion acceleration (Giacalone 2005a,b) since particle transport normal to the mean field is enhanced. However, the particle transport in full 3-D turbulence can not be properly treated in a self-consistent way using available computation. As demonstrated by previous works (Jokipii, Kota & Giacalone 1993; Giacalone & Jokipii 1994; Jones et al. 1998), in the model with at least one ignorable coordinate, the center of gyration of particles is confined to within one gyroradius of the original magnetic field line. The test-electrons can still move normal to the mean field in our model because of the field-line random walk.

In the second part of our calculation we integrate the full motion equation of an ensemble of test-particle electrons in the electric and magnetic fields obtained in the hybrid simulations (see Figure 1). This part of the calculation is done separately from the main hybrid simulation as a post processing phase. We assume non-relativistic motion which is reasonable because the highest energy electrons obtained in our study are still non-relativistic. As noted by Krauss-Varban et al. (1989), high-order interpolation of fields is required to ensure numerical accuracy and avoid artificial scattering in calculating electron trajectories. In this work we use second-order spatial interpolation and linear temporal interpolation, which ensure the smooth variations of the electromagnetic fields. We release a shell distribution of electrons with energy of 100 eV, which corresponds to an electron velocity $V_e = 30.7U_1 = 5.7v_{the}$ in the upstream frame, where U_1 is upstream bulk velocity in the shock frame and v_{the} is the thermal velocity of fluid electrons considered in the hybrid simulations, respectively. This energy is typical for the halo component of electron velocity distributions observed in solar wind. The test-particle electrons are released uniformly upstream at $t = 70\Omega_{ci}^{-1}$ when the shock has fully formed and is far from the boundaries. The numerical technique used to integrate electron trajectories is the so-called Bulirsh-Stoer method, which is described in detail by Press et al. (1986). It is highly accurate and conserves energy well. It is fast when fields are smooth compared

with the electron gyroradius. The algorithm uses an adjustable time-step method based on the evaluation of the local truncation error. The time step is allowed to vary between 5×10^{-5} and $0.1\Omega_{ce}^{-1}$, where Ω_{ce} is the electron gyrofrequency. The ratio Ω_{ce}/Ω_{ci} is taken to be the realistic value 1836. The total number of electrons in the simulation is 1.6×10^6 . The electrons which reach the left or right boundary are assumed to escape from the shock region and are removed from simulation. The boundary condition in the z direction is taken to be periodic. The readers are referred to (Burgess 2006) for more details on the numerical methods.

Magnetic field turbulence has already been proved to have key effect on the particle acceleration in collisionless shocks. Unfortunately, solving the whole problem in three-dimensional space and resolving magnetic turbulence from coherence scale to electron scale are still limited by available computation in the near future. This limitation motivates us to solve these problems approximately. We also note that in our model the electron test particle simulation is not self-consistent since the hybrid simulation does not include the electron scale physics. The electron scale shock structure, which may be important is neglected here.

3. Simulation Results

Figure 1 shows a snapshot of the z component of the magnetic field, B_z/B_1 , at time $110\Omega_{ci}^{-1}$ in a gray-scale representation, overlaid by a two-dimensional magnetic vector field. At this time, the shock is fully developed. In this case, the angle between the average magnetic field direction and shock normal, $\langle \theta_{Bn} \rangle$ is 90° . The position of the shock front is clearly seen from the boundary of the magnetic field jump. The shock is moving in the $-x$ direction at a speed dependent on z , which is about $1.6 v_{A1}$ on average. Because of the effect of large-scale turbulence with the shock, the shock surface become irregular on a variety of

spatial scales from small-scale ripples, which could be due to ion-scale plasma instabilities (Lowe & Burgess 2003), to large-scale structure caused by the interaction between the shock and upstream turbulence (Neugebauer & Giacalone 2005; Giacalone & Neugebauer 2008; Lu et al. 2009). The upstream magnetic field is compressed and distorted as it passes through the shock into the downstream region. We note that the rippling of the shock and varying upstream magnetic field leads to a varying local shock normal angle along the shock front. As we will discuss later, the irregular shock surface and magnetic field geometry will efficiently accelerate electrons and produce a number of features similar to observations, such as the electron foreshock and spike-like intensity increases at the shock front. The meandering of field lines close to the shock surface helps to trap the electrons at the shock, leading to efficient acceleration. The shock ripples also contribute to the acceleration by mirroring electrons between them.

Figure 2 shows a color-coded representation of the number of energetic electrons with energies higher than 10 times (i.e., 1 keV) the initial (at release) energy at three different times (a) $76\Omega_{ci}^{-1}$, (b) $81\Omega_{ci}^{-1}$, (c) $90\Omega_{ci}^{-1}$, respectively. It is found that after the initial release, a fraction of the electrons are reflected and accelerated at the shock front, and then travel upstream along the turbulent magnetic field lines. These accelerated electrons are then taken back to the shock by the field line meandering, which provides even further acceleration. The number of energetic electrons close to the shock surface is highly irregular because the acceleration efficiency varies along the shock front depending on the local shock normal angle (Wu 1984). Most of the electrons are concentrated near the shock front since the global magnetic field is mostly perpendicular to the shock normal. As the field lines convect through shock, the electrons eventually are taken downstream. Since the electrons are tied to individual field lines in 2-D magnetic field, once the electrons are no longer capable of crossing the shock, there will be no additional significant acceleration. At this point, once all electrons are downstream, the energy spectrum no longer changes with time.

Examination of the trajectories of some electrons shows that the rippling of the shock front also contributes to the acceleration by mirroring electrons between the ripples, as illustrated in Figure 3. In this figure, the top left plot displays the trajectory of a representative electron in the $x - z$ plane, overlapped with the 2-D gray-scale representation of B_z at $\Omega_{ci}t = 89.0$, the gray scale is the same as in Figure 1. The upper right plot shows the position of this electron (in x) as a function of time. The electron bounces back and forth between the ripples for several times. For example, the reflections are labeled $a - b$, c , d , $f - g$, h , and j . The energy change as a function of position, x , corresponding to these reflections is shown in the bottom left panel. We find that there are jumps in energy at each of the reflections. The panel on the bottom right shows the electron energy as a function of time which also illustrates the features of multiple accelerations related to multiple reflections. The trajectory analysis shows the electron will be mirrored between the ripples for a couple of times and by this get accelerated multiple times. Note that the shock does not move much during the time scale of this trajectory.

We now consider the effect of varying the angle between the mean magnetic field and shock-normal. Shown in Figure 4 are the resulting energy spectra for three different mean shock-normal angles ($\langle \theta_{Bn} \rangle = 60^\circ, 75^\circ$ and 90° , respectively) at the end of simulations ($\Omega_{ci}t = 120.0$). It is found that for $\langle \theta_{Bn} \rangle = 90^\circ$, the electrons can readily be accelerated to up to 200 – 300 times the initial energy within $50\Omega_{ci}^{-1}$. The spectrum is flat between about 0.1 keV to 0.7 keV. This shape is similar to the "plateau" structure discussed by Burgess (2006). Above 1 keV, the spectrum falls off with energy as a slope index about -3 . It can be found that both the number fraction and highest energy of accelerated particles decreases as $\langle \theta_{Bn} \rangle$ decreases. We have also tried different value of initial energies (not shown), and find that the acceleration efficiency decreases for electrons with higher initial energies, which is similar to the results of (Burgess 2006).

The effect of different strengths of magnetic turbulence is examined in Figure 5. We compare three cases with different turbulence variances $\sigma = 0.1, 0.3, \text{ and } 0.5$, respectively. At the end of simulations, the final energy spectra are similar at low energies, with significant variations in the spectra only at energies larger than 2 keV. It is found that the energy spectrum is hardened at high energies when the turbulence variance is largest, which indicates the large-scale turbulence is more important for accelerating electrons to high energies. We argue that collisionless shocks which move through magnetic turbulence with significant power leads to efficient electron acceleration to high energies since the motion normal to the shock front is enhanced. The reason is that the meandering of field lines is enhanced, which allows the electrons have a better chance to travel through the shock multiple times.

We note that the spatial distribution of energetic electrons is determined not only by the ripples in the shock front, but also by the global topology of the magnetic field lines. An example is shown in Figure 6, which shows the profiles of the number of energetic electrons at $\Omega_{ci}t = 100.0$ as a function of x , for the case of $\langle \theta_{Bn} \rangle = 90^\circ$. The black solid line is the profile at $z = 200c/\omega_{pi}$, and the red dash line shows the profile at $z = 800c/\omega_{pi}$. The corresponding position of the shock front at each of these values of z are represented using dot lines. At $z = 200c/\omega_{pi}$, it is observed that the energetic electrons travel far upstream up to about $100c/\omega_{pi}$. However, the profile at $z = 800c/\omega_{pi}$ shows no significant upstream energetic electron flux. The upstream energetic electron profiles show irregular features similar to in-situ observations reported by Simnett et al. (2005) (in Figure 10). The irregular features are controlled by the global topology of the large-scale turbulent magnetic field lines, along which the accelerated electrons could travel far upstream. Additionally, energetic electron profiles in x direction generally show "spike-like" structure close to the shock front, which is usually observed in interplanetary shocks and Earth's bow shock. We note this feature is relatively stable within the simulation time once the upstream electron

structure developed.

4. Discussion and Conclusions

We studied the acceleration of electrons at collisionless shocks by utilizing a combination of a 2-D hybrid simulation to obtain the shock structure and a test-particle simulation to determine the motion of electrons. The hybrid simulation provides realistic electric and magnetic fields within the transition layer of the shock that effect the motion of test-electrons, which is determined by solving the equation of motion. The interaction of the shock with pre-existing upstream fluctuations, and other nonlinear processes occuring in the hybrid simulation lead to a "rippling" of shock surface which also effects the transport of the electrons.

We find that the electrons are efficiently accelerated by a nearly perpendicular shock. The turbulent magnetic field, leads to field-line meandering which allows the electrons to cross the shock front many times. The rippling of the shock front also contributes to the acceleration by mirroring electrons between the ripples. For the case that the averaged shock normal angle $\langle \theta_{Bn} \rangle = 90^\circ$ and turbulence variance $\sigma = 0.3$, the electrons can readily be accelerated to up to 200 – 300 times the initial energy. The resulting spectrum is flat between about 0.1 keV to 0.7 keV. At higher energies, the spectrum falls off with energy like a power law with a spectral slope of about -3 . This acceleration process is more efficient at perpendicular shocks. As $\langle \theta_{Bn} \rangle$ decreases from 90° , both the number fraction and highest achievable energy of accelerated particles decreases. Based on our calculations, we conclude that perpendicular shocks are the most important for the acceleration of electrons. The current study is helpful in understanding the injection problem for electron acceleration by collisionless shocks. It is also found that different value of magnetic turbulence variances strongly affects the maximum energy attainable. The case with larger turbulence variance

has a flatter energy spectrum than the case of smaller turbulence variance, which suggests the enhanced motion of electrons normal to the shock front, due to enhanced field-line random walk, is of importance for the acceleration of electrons to high energies.

In addition, we also found that the energetic electron density upstream and downstream of collisionless shocks show filamentary structures (Figure 2). This could help explain electron spike-like events observed upstream and downstream of terrestrial and interplanetary shocks (Anderson et al. 1979; Tsurutani & Lin 1985; Simnett et al. 2005). Observation by Voyager 1 at the termination shock and in the heliosheath also show the evidence of electron spike-like enhancements at the shock front (Decker et al. 2005). The upstream spatial distribution of energetic electrons shows irregular features which depend on both the irregularity in the shock surface and the global topology of magnetic field lines. At first the electrons are accelerated and reflected at the shock front, and then they travel upstream along the magnetic field lines. The electrons could be taken far upstream by field line random walk. This result can possibly lead to an interpretation to the complex electron foreshock events recently observed to be associated with interplanetary shocks (Bale et al. 1999; Pulupa & Bale 2008). Bale et al. (1999) and Pulupa & Bale (2008) proposed the complex upstream electron events are resulted from large-scale irregularities in shock surface. In this paper we have demonstrated that the upstream electron flux may be controlled by both an irregular shock surface and large-scale meandering magnetic field lines.

Acknowledgement

The authors would like to thank Dr. D. Burgess for sharing the details of numerical methods and Dr. J. R. Jokipii for valuable discussions. This work was supported in part by NSF under grant ATM0447354 and by NASA under grant NNX07AH19G.

REFERENCES

- Anderson, K. A., Lin, R. P., Martel, F., Lin, C. S., Parks, G. K., & Reme, H. 1979, *Geophys. Res. Lett.*, 6, 401
- Axford, W. I., Leer, E., & Skadron, G. 1978, *Proc. 15th Int. Cosmic-Ray Conf. (Plovdiv)*, 132
- Armstrong, T. P., Pesses, M. E., Decker, R. B. 1985, *Shock Drift Acceleration, Collisionless Shocks in the Heliosphere: A Tutorial Review*, AGU Geophysical Monograph Series, 35, 271
- Bale, S. D., Reiner, M. J., Bougeret, J.-L., Kaiser, M. L., Krucker, S., Larson, D. E., & Lin, R. P. 1999, *Geophys. Res. Lett.*, 26, 1573
- Ball, L., & Melrose, D. B. 2001, *Publ. Astron. Soc. Australia*, 18, 361
- Bell, A. R. 1978, *MNRAS*, 182, 147
- Blandford, R. D., & Ostriker, J. P. 1978, *ApJ*, 221, L29
- Burgess, D., 2006, *ApJ*, 653, 316
- Decker, R. B. 1988, *Space Sci. Rev.*, 48, 195
- Decker, R. B., Krimigis, S. M., Roelof, E. C., Hill, M. E., Armstrong, T. P., Gloeckler, G., Hamilton, D. C., & Lanzerotti, L. J. 2005, *Science*, 309, 2020
- Giacalone, J., Burgess, D., Schwartz, S. J., & Ellison, D. C. 1992, *Geophys. Res. Lett.*, 19, 433
- Giacalone, J., & Jokipii, J. R. 1994, *ApJ*, 430, L137
- Giacalone, J. 2004, *ApJ*, 609, 452

Giacalone, J. 2005a, ApJ, 624, 765

Giacalone, J. 2005b, ApJ, 628, L37

Giacalone, J., & Neugebauer, M. 2008, ApJ, 673, 629

Holman, G. D., & Pesses, M. E. 1983, ApJ, 267, 837

Jokipii, J. R., Kota, J., and Giacalone, J., 1993, Geophys. Res. Lett., 20, 1759

Jokipii, J. R., & Giacalone, J. 2007, ApJ, 660, 336

Jones, F. C., & Ellison, D. C. 1991, Space Sci. Rev., 58, 259

Jones, F. C., Jokipii, J. R., & Baring, M. G. 1998, ApJ, 509, 238

Krauss-Varban, D., Burgess, D. and Wu, C. S., 1989, J. Geophys. Res., 94, A11, 15089-15098

Krauss-Varban, D., & Wu, C. S. 1989, J. Geophys. Res., 94, 15367

Krymsky, G. F. 1977, Dokl. Akad. Nauk SSSR, 234, 1306

Lee, M. A., Shapiro, V. D., & Sagdeev, R. Z. 1996, J. Geophys. Res., 101, 4777

Leroy, M. M., and Mangeney, A., Ann. Geophys., 2, 449-456, 1984

Lowe, R. E., & Burgess, D. 2003, Ann. Geophys., 21, 671

Lu Q., Hu, Q. and Zank, G. P., 2009, ApJ 706, 687

Neugebauer, M., & Giacalone, J. 2005, J. Geophys. Res., 110, 12106

Ng, C. K., Reames, D. V., & Tylka, A. J. 2003, ApJ, 591, 461

Press, W. H., Flannery, B. P., Teukolsky, S. A., & Vetterling, W. T. 1986, Numerical Recipes (Cambridge: Cambridge University Press)

Pulupa, M., & Bale, S. D. 2008, *ApJ*, 676, 1330

Sagdeev, R. Z. 1966, *Rev. Plasma Phys.*, 4, 23

Shimada, N., Terasawa, T., Hoshino, M., Naito, T., Matsui, H., Koi, T., & Maezawa, K.
1999, *Ap&SS*, 264, 481

Simnett, G. M., Sakai, J.-I., & Forsyth, R. J. 2005, *A&A*, 440, 759

Tsurutani, B. T., & Lin, R. P. 1985, *J. Geophys. Res.*, 90, 1

Winske, D., & Quest, K. B. 1988, *J. Geophys. Res.*, 93, 9681

Wu, C. S., 1984, *J. Geophys. Res.*, 89, 8857

Zank, G. P., Pauls, H. L., Cairns, I. H., & Webb, G. M. 1996, *J. Geophys. Res.*, 101, 457

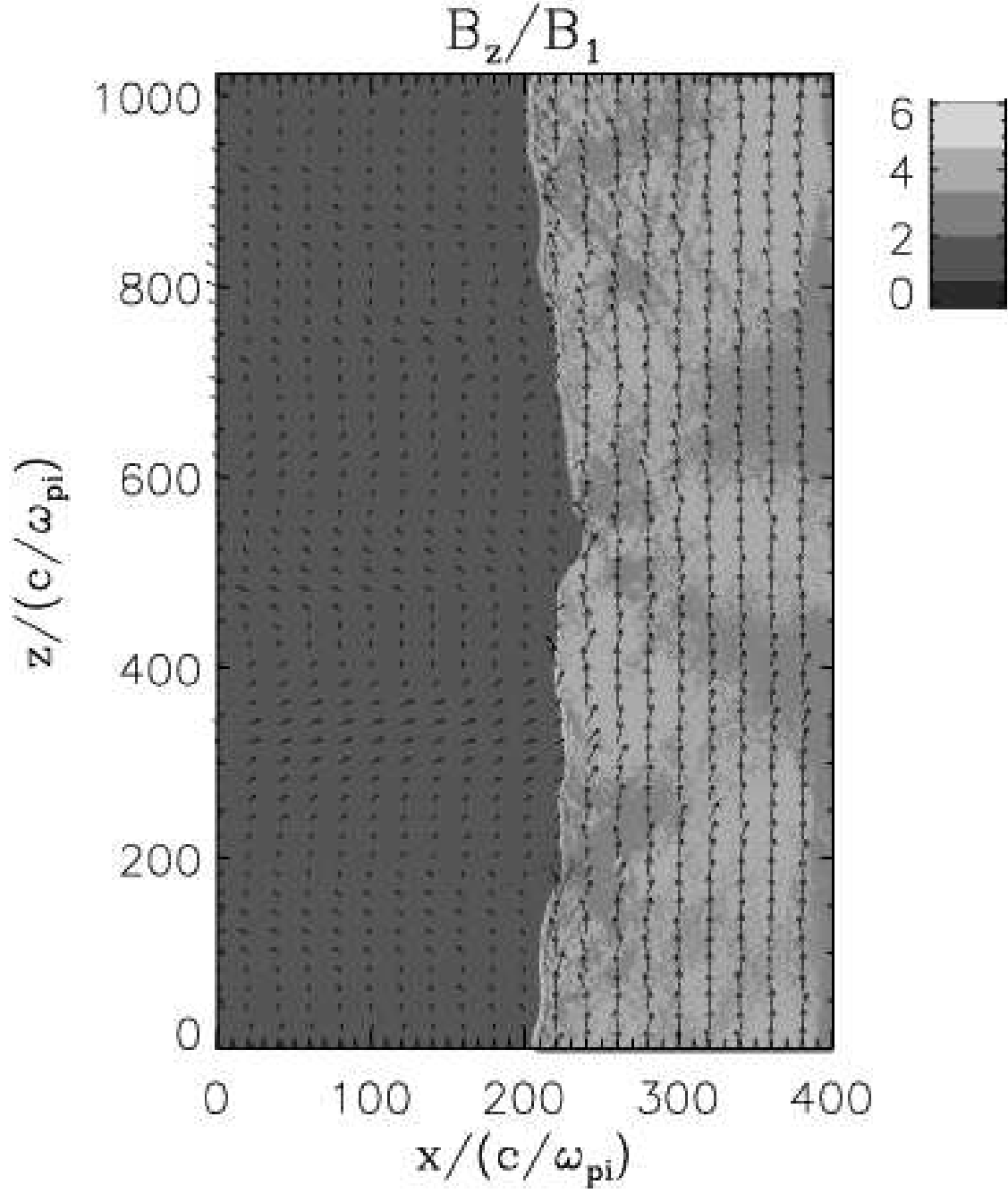


Fig. 1.— A snapshot of magnetic field in z direction B_z/B_1 represented in gray-scale at time $110\Omega_{ci}^{-1}$, where B_1 is the averaged upstream magnetic field strength. A two-dimensional vector field is also overlapped, which indicates the direction of magnetic field. The shock surface is shown to be rippled and irregular in different scales.

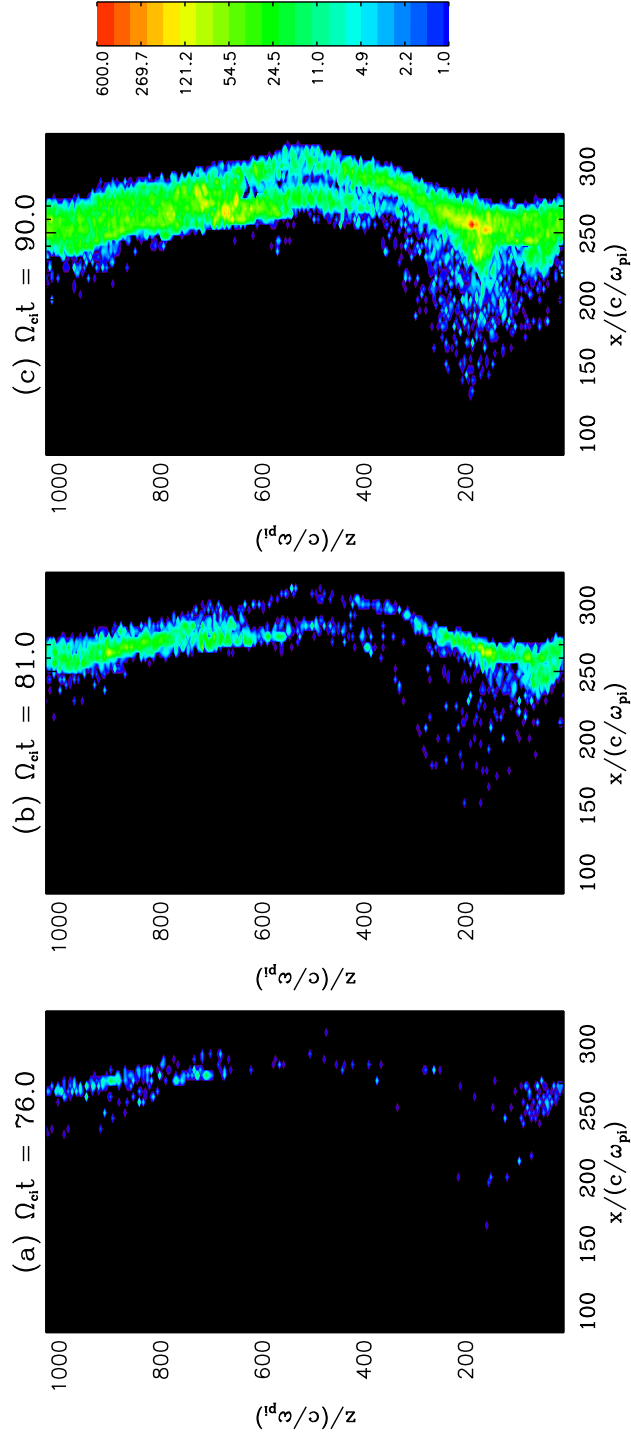


Fig. 2.— The number of energetic electrons with energies $E > 10E_0$, the initial release energy $E_0 = 100$ eV, at (a) $\Omega_{ci}t = 76$, (b) $\Omega_{ci}t = 81$, and (c) $\Omega_{ci}t = 90$, respectively. Initially electrons are released uniformly upstream at $\Omega_{ci}t = 70$.

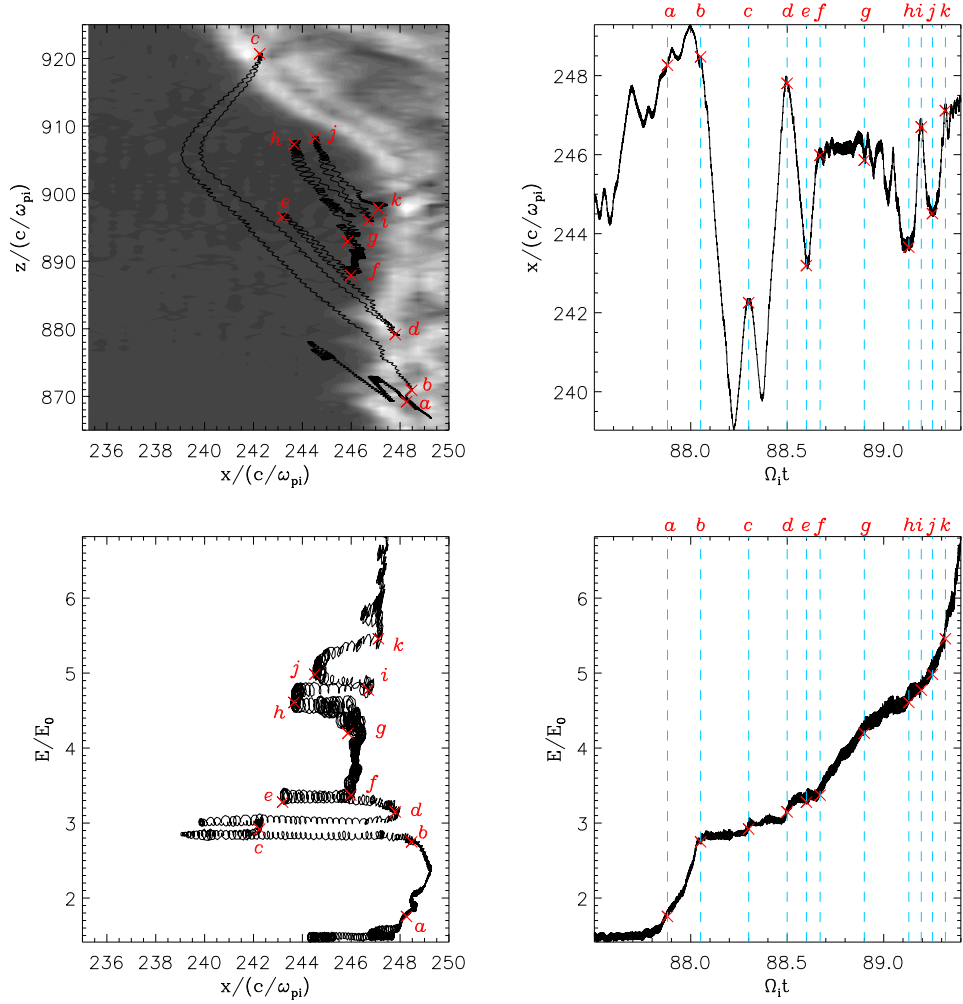


Fig. 3.— A typical electron trajectory analysis which shows acceleration by multiple mirroring between ripples. The top left panel displays the trajectory of the representative electron in $x - z$ plane, overlapped with contour of B_z magnetic field where the gray-scale is the same as that in Figure 1; The top right panel shows the position of the electron in x coordinate as a function of time; The bottom left panel illustrates the energy of the representative electron E/E_0 as a function of x ; The bottom right panel shows the dependence of electron energy E/E_0 on time.

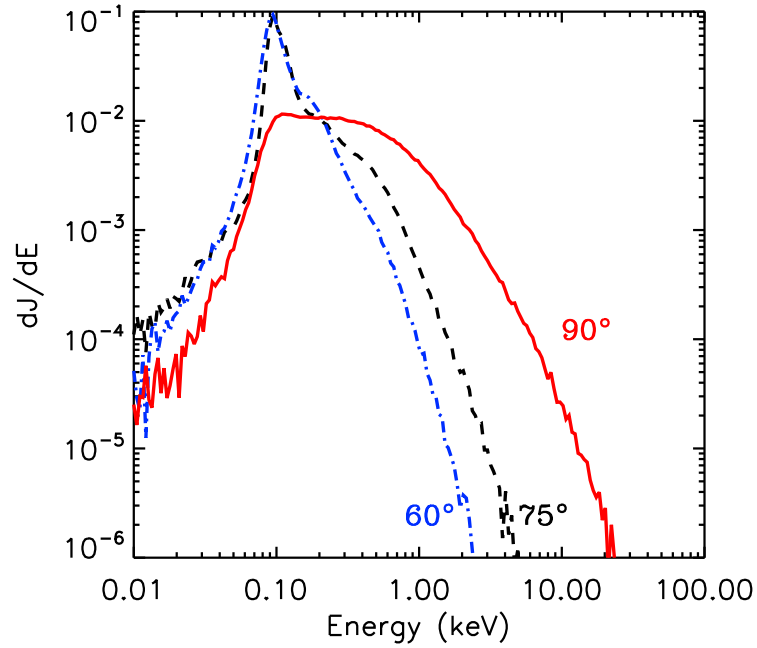


Fig. 4.— The energy flux spectrum of electrons at $\Omega_{ci}t = 120$ for different averaged shock normal angle. The red solid line is in the case that the shock angle $\langle \theta_{Bn} \rangle = 90^\circ$, the blue dot dashed line and the black dashed line are in the cases that $\langle \theta_{Bn} \rangle = 60^\circ$ and 75° , respectively.

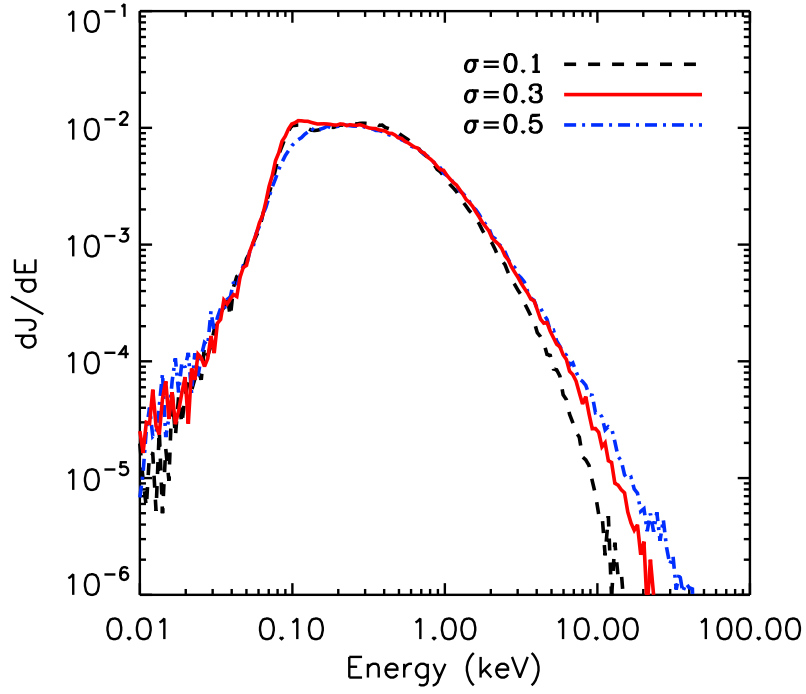


Fig. 5.— The energy flux spectrum of electrons at $\Omega_{ci}t = 120$ for averaged perpendicular shock with different turbulence variances. The black dashed line, red solid line, and blue dot dashed line are in the cases that $\sigma = 0.1, 0.3,$ and $0.5,$ respectively.

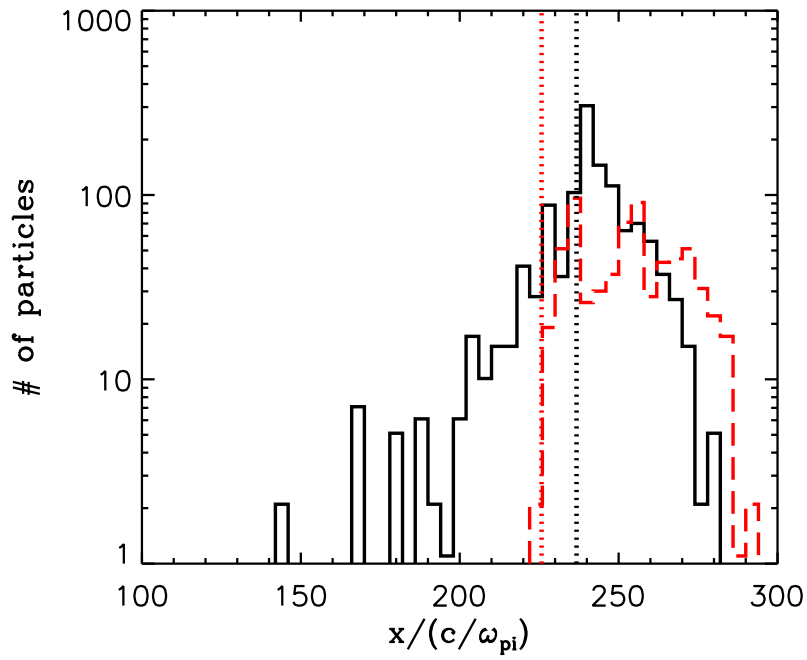


Fig. 6.— The solid black line and dashed red line show the profiles of the number of energetic electrons at $z = 200c/\omega_{pi}$ and $z = 800c/\omega_{pi}$ at time $\Omega_{ci}t = 100$, respectively. The red dot line and black dot line label the corresponding positions of the shock fronts.